

Visualizing high-temperature spin dynamics in $\text{La}_{1-x}\text{Ca}_x\text{MnO}_3$

from a mapping of EPR linewidth and g factor

Y. Liu* and S. L. Wan

*Department of Modern Physics, University of Science and Technology of China,
Hefei 230026, P. R. China*

X. G. Li

*Hefei National Laboratory for Physical Sciences at Microscale, Department of Physics,
University of Science and Technology of China, Hefei 230026, P. R. China*

Abstract

We report the measurements of electron paramagnetic resonance (EPR) on powder samples of $\text{La}_{1-x}\text{Ca}_x\text{MnO}_3$ at the commensurate carrier concentrations of $x = N/8$ ($N = 1, 2, 3, 4, 5, 6$, and 7) within temperature range $100\text{K} \leq T \leq 450\text{K}$. It is suggested that the mapping of EPR linewidth and g factor is a useful way to reveal the high-temperature spin dynamics in $\text{La}_{1-x}\text{Ca}_x\text{MnO}_3$. An electron-hole asymmetry can be clearly observed in the mapping of g factor. The linewidth ΔH as a function of x drops at $x = 3/8$ due to the mechanism of exchange narrowing. The activation energy ΔE obtained by fitting the intensity I to an Arrhenius law displays a sharp peak at $x = 3/8$, suggesting a strong ferromagnetic coupling. Our results convince that the spin-only relaxation mechanism should dominate the high-temperature paramagnetic regime in colossal magnetoresistance (CMR) manganites.

PACS number(s): 75.47.Lx, 76.30.-v, 71.38.Ht

* Corresponding author. Email address: yliu@ustc.edu.cn

Due to a complex interplay among charge, spin, orbital, and lattice degrees of freedom, doped perovskite manganites $R_{1-x}A_xMnO_3$, where R is a trivalent rare earth ion and A is a divalent alkaline earth ion, show a rich phase diagram as a function of doping, temperature, and magnetic field [1-3]. The prototypical manganite system is $La_{1-x}Ca_xMnO_3$ (LCMO), which exhibits various ground states with the variation of carrier concentration. The phase diagram of LCMO was studied through the measurements of magnetization, resistivity, thermal conductivity, and thermopower by Cheong and co-workers in detail [4]. It is generally accepted that the competition between the double exchange (DE) interaction [5] and an enhanced electron-phonon coupling via the Jahn-Teller (JT) active Mn^{3+} ion [6] plays a key role in determining the phase diagram of the manganites. A qualitative picture to explain the phase diagram of LCMO can be summarized: In samples with $0.2 < x < 0.5$, a transition from paramagnetic insulating (PI) to ferromagnetic metallic (FM) state occurs upon cooling due to the predominant DE mechanism. For the higher doping range with $0.5 < x < 0.875$ the ground state favors a charge ordering (CO) state. It was shown that the dominant mechanism responsible for the charge order is the JT coupling, with a lesser but significant contribution from the on-site Coulomb interaction [7]. In contrast to rich doping dependent ground states, high-temperature PI regime above the ordering temperatures seems to be simply dominated by the self-trapped small polarons [6,8]. X-ray and neutron scattering measurements have directly demonstrated the presence of short-range polaron correlations in the PI phase of optimally doped manganites [9-11]. Surprisingly, the ground state of $La_{5/8}Ca_{3/8}MnO_3$ is FM phase, but the insulating nature of the system above the Curie temperature T_C is correlated with nano-scale charge/orbital ordering [12]. The results strongly suggest that the PI regime in LCMO phase diagram is more complicated than one's intuition thinking.

From the experimental point of view, much effort has been devoted to understand magnetic, electrical transport, and thermal properties in the paramagnetic state [8]. In these

studies magnetic correlations are supposed to be completely ignored, since electron-phonon and on-site Coulomb interactions dominate in the high-temperature regime. However, one can not exclude the role of magnetic correlations when considering short-range polaron correlations. An analysis of the spin-spin correlations based on the Monte Carlo calculations shows that the ferromagnetic clusters form with size to be three-to-four lattice spacings above T_C [13]. The short-range CO correlation at high temperature is possibly in the form of a FM “zigzag,” a small segment of the CE-type CO state [12].

The main purpose of this study is to depict spin dynamics in the PI regime of LCMO phase diagram. The electron paramagnetic resonance (EPR) is a powerful probe of spin dynamics in the manganites. We report a systematic investigation of the temperature dependences of the EPR line resonance field (g factor), linewidth ΔH , and intensity I for polycrystalline samples of LCMO at the commensurate carrier concentrations of $x = N/8$ ($N = 1, 2, 3, 4, 5, 6$, and 7). As is evident in the phase diagram, there are well defined features at the commensurate carrier concentrations of $x = N/8$ ($N = 1, 3, 4, 5$, and 7) in LCMO [4], e.g., optimal doping for FM state at $x = 3/8$, the highest CO temperature T_{CO} at $x = 5/8$. Moreover, Curie temperature T_C is similar to the temperature T_{CO} for the two doping levels, forming an electron-hole symmetry phase line centered at $x = 4/8$.

High-quality polycrystalline samples LCMO with commensurate doping of $x = N/8$, ($N = 1\sim 7$) were prepared by a standard solid-state reaction with an identical synthesis condition. Stoichiometric proportions of La_2O_3 , CaCO_3 , and MnCO_3 were mixed and heated at $1200\text{ }^\circ\text{C}$ for two days with an intermediate grinding. After grinding, the mixture was pressed into pellets and sintered at $1300\text{ }^\circ\text{C}$ for 24 h. Phase purity and crystal structure of the samples were characterized by x-ray diffraction (XRD). Figure 1 shows the Ca doping dependence of XRD patterns for LCMO ($x = N/8$, $N = 1\sim 7$) at room temperature, which could be indexed in a *Pnma*-type orthorhombic structure. The EPR spectra were recorded using a Bruker ER200D

spectrometer at 9.61 GHz (*X* band) upon warming within the temperature range $100\text{K} \leq T \leq 450\text{K}$. The measurements were carried out on loose-packed micron-sized crushed crystals.

Figure 2 shows the EPR spectra recorded as the derivative dP/dH at room temperature for the samples. Each ESR spectra consists of a symmetric Lorentzian line. Oseroff *et al.* [14] suggested that the EPR signal in the manganites is a consequence of magnetic clusters made of a collection of Mn^{3+} and Mn^{4+} ions. In the EPR measurements, the parameters of primary interest are the *g* factor and the linewidth ΔH . Since the lines are very broad both in powder and single crystals, for accurate determination of the various line shape parameters we have fitted the signals to appropriate line shape functions. For powder samples small compared to the skin depth, one expects a symmetric absorption spectrum [15]

$$\frac{dP}{dH} \propto \frac{d}{dH} \left(\frac{\Delta H}{(H - H_r)^2 + \Delta H^2} + \frac{\Delta H}{(H + H_r)^2 + \Delta H^2} \right), \quad (1)$$

where H_r is the resonance field and ΔH is the linewidth. As shown in Fig. 2, the fits of the signals to Eq. (1) are excellent.

From the best fit value of the resonance field H_r , the *g* value is obtained from the resonance condition: $h\nu = g\mu_B H_r$. Figure 3(a) plots the temperature dependence of *g* value for the samples. It is found that the *g* values are nearly temperature independent except those close to the ordering temperatures. Interestingly, *g* values divide into two distinct parts for the hole doped and electron doped samples. By linearly interpolating the results, we can draw a false color mapping of *g* factor in the T vs x , as shown in Fig. 3(b). It is noteworthy that *g* factor displays an electron-hole asymmetry forming a phase line centered at $x = 4/8$. The feature of electron-hole asymmetry was also observed in $\text{Pr}_{1-x}\text{Ca}_x\text{MnO}_3$ (PCMO), where the *g* value for the electron doped sample ($x = 0.64$) is less than the free electron value $g_e \sim 2.0023$, whereas for the hole doped one ($x = 0.36$) it is more than g_e at room temperature [16]. In

powder samples the individual grains are randomly orientated. The local field has little influence on the resonance field, leaving the g value unaffected. Thus we believe the electron-hole asymmetry of g factor is an intrinsic phenomenon.

Values of g for a formal orbitally singlet ground state can be expressed by $g = g_e(1 - k\lambda/\Delta)$, where λ is the effective spin-orbit coupling constant, Δ is the energy gap between the ground level and the excited level in question, and k is a constant depending on the two levels concerned [17]. Thus, the g value may afford information about the effective value of λ and the energy gap Δ . The former has been interpreted to give a measure of covalency of the bond between the central metal ion and the ligands. In the phase diagram of LCMO the ground state is a FM phase within the temperature range $0.2 < x < 0.5$, while for $x > 0.5$ the CO state is stabilized at low temperatures. The low-energy optical conductivity in the PI state of the optimally doped sample is characterized by a broad maximum near 1 eV attributed to the hopping motion of small polarons. This feature remains identifiable well below T_C and transforms eventually into a Drude-like response [18,19]. On the other hand, an optical gap due to the long-range CO, namely, a charge gap, is clarified in electron doped samples [20]. This charge gap is 0.45 eV for both $x = 0.50$ and 0.52 samples, and decreases rapidly with increasing x . If we assume λ and k are slowly varying functions of x , the electron-hole asymmetry of g factor can be explained modestly.

In contrast to g factor, the linewidth ΔH for the samples show a wide variety of behaviors depending on both the temperature and doping level, as shown in Fig. 4(a). As a function of T , the EPR linewidth ΔH for all the samples except $x = 7/8$ decreases with decreasing temperature. The linewidth ΔH of the sample $x = 7/8$ saturates rapidly with increasing temperature. Upon cooling ΔH in all cases goes through a minimum at T_{\min} . Below this temperature ΔH increases rapidly. It was reported that this behavior is not intrinsic but extremely sample dependent [21]. The feature can be well described in terms of a

two-magnon scattering relaxation mechanism induced by the demagnetization fields of the pores between crystallites. Since the behavior observed between the ordering temperatures and T_{\min} is sample dependent and may confuse the analysis of the results in the paramagnetic regime, we have excluded this small temperature region from our analysis.

We show the mapping of the EPR linewidth in Fig. 4(b). Remarkably, on approaching the ordering temperatures from above, the narrowing of EPR linewidth gets strong for $x \leq 0.5$, where colossal magnetoresistance (CMR) effect is observed. It is found that the narrowing of EPR linewidth is strongly correlated with T_C . The linewidth ΔH is the narrowest for the optimally doped sample $x = 3/8$ at the same temperature. The drop of ΔH extends to the highest temperature, related to the highest Curie temperature T_C at this doping level. Let's turn to the resistivity ρ at 300 K for LCMO [4]. Note at 300 K the smooth behavior as x grows from 0, only interrupted close to $x = 1$ when the G-type antiferromagnetic insulating (AFI) state is reached. It was found that, however, doping dependence of magnetic susceptibility χ at 300 K display a strikingly sharp peak at $x = 3/8$ composition [12]. According to Zener's DE mechanism [5], e_g electrons hop between Mn^{3+} and Mn^{4+} ions while keeping their spin directions due to a strong Hund coupling energy because such hopping is most probable when the spins of t_{2g} electrons of the Mn^{3+} are aligned with those of the adjacent Mn^{4+} . Thus, the enhancement of FM correlation is related to the strongest exchange interactions at $x = 3/8$.

It is well known that in a paramagnet where the nearest neighbouring spins are coupled by an exchange interaction J , the EPR signal should be strongly exchange narrowed so that instead of the full dipolar width ΔH_0 [22]. One should observed a linewidth

$$\Delta H = (\Delta H_0)^2 / \Delta H_{\text{ex}} \quad (2)$$

where ΔH_{ex} is the exchange field. ΔH_{ex} is quite large and related to the Curie temperature ($S\mu_B\Delta H_{\text{ex}} \approx k_B T_C$). Thus the drop of linewidth ΔH at $x = 3/8$ can be roughly interpreted in terms of exchange narrowing when leaving the dipolar fields unchanged [23]. It has been

found that the polaronic state near the optimal doping is intrinsically inhomogeneous, consisting of magnetic clusters 10 to 20 Å in diameter [9-12]. Generally, the polaronic state is a consequence of the strong electron-phonon coupling, enhanced by the JT activity of Mn^{3+} ion in the manganites. On the other hand, the exchange correlation is strongly enhanced for x near 3/8, which is relevant for the presence of short-range polaron correlations. Our observation naturally suggests that the exchange correlation provides the “glue” for the formation of FM coupled polarons. This result presents great implications on the origin of the EPR signal in the manganites. It seems reasonable to identify short-range correlated polarons with the spin entity suggested by Oseroff *et al.* [14].

It is still a controversial issue on the relaxation mechanism for the temperature dependence of linewidth ΔH in the manganites. The linewidth ΔH shows a linear T dependence between $1.1T_C < T < 2T_C$ for hole doped manganites, which was interpreted in terms of a single-phonon spin-lattice relaxation mechanism [23,24]. By substituting ^{16}O for ^{18}O , the characteristic differences observed in EPR intensity and linewidth for the two isotope samples were suggested to be caused by a bottlenecked spin relaxation takes place from the exchange-coupled constituent Mn^{4+} ions via the Mn^{3+} Jahn-Teller ions to the lattice [25]. Further, Shengelaya *et al.* [26] found that the temperature dependence of linewidth ΔH can be described by the adiabatic hopping of small polarons, *i.e.*, $\sigma \propto T^{-1} \exp(-E_a / k_B T)$, which is consistent with the existence of a bottleneck EPR regime in the manganates. We have fitted our data show in Fig. 4(a) by the following expression

$$\Delta H = \Delta H_0 + \frac{A}{T} \exp(-E_a / k_B T), \quad (3)$$

where E_a is the activation energy, *i.e.*, the potential barrier that the polaron must surmount in order to hop into the next site. The E_a values obtained by fitting Eq. (3) are plotted in Fig. 5(a). The data obtained in the previous work at $x = 0.18, 0.2$, and 0.22 are also presented in Fig. 5(a)

[26,27]. It is found that E_a values display a peak at $x = 3/8$. However, E_a values deduced from the conductivity measurements show a striking divergence from those measured by EPR technique. As shown in Fig. 5(a), they decrease smoothly with increasing x [28]. No anomalous behaviors are observed at $x = 3/8$. As can be seen in Fig. 5(a), the coincidence of E_a values only occurs around $x = 1/3$ and $5/8$. On the other hand, Atsarkin *et al.* [29] have measured the longitudinal spin-relaxation time T_1 in the paramagnetic state of three LCMO samples ($x = 0.2$, 0.25 , and 0.33). The reported T_1 behavior contradicts that predicted by the polaron model.

According to Ref. 25, the EPR signal observed in LCMO is due primarily to Mn^{4+} ions. It was found that, however, both Mn^{4+} and Mn^{3+} ions take part in producing the EPR signal [23]. A further study suggest that EPR susceptibility χ_{esr} , deduced from the relation $I \propto \chi_{\text{esr}}$ (I is EPR intensity), could be identified with magnetic susceptibility χ_{dc} [30]. The EPR experiment probes the dynamics of the magnetic system. The coincidence of $\chi_{\text{esr}}(T)$ with $\chi_{\text{dc}}(T)$ in the whole PI range studied clearly indicates that all the Mn ions contribute to the observed EPR spectra. Thus, the EPR linewidth should be related to the relaxation mechanism of the coupled magnetic system. In this study, the EPR intensity I was determined by numerical double integration of the measured spectra. Instead of a simple Curie-Weiss law, the intensity I during PI regime follows an Arrhenius law [13,14,30],

$$I = I_0 \exp(\Delta E / k_B T), \quad (4)$$

where ΔE is the activation energy of spin clusters. Since the EPR signal is associated with some form of the magnetic cluster [14], the ΔE would be required in order to dissociate these spin entities made of collection of individual spins [13]. Figure 5(b) shows ΔE obtained by a linear fit of $\ln I$ vs $1000/T$ plots. Interestingly, the activation energy ΔE resembles the result obtained by fitting linewidth ΔH with Eq. 3, and peaks at $x = 3/8$. This feature was also observed by Oseroff *et al.* [14]. The peaking behavior of ΔE should be related to the strong

FM coupling at $x = 3/8$ [12].

In any case, the nature of the EPR broadening is determined by the mechanism of the electron spin relaxation. According to Refs. 30-32, the EPR linewidth in a wide variety of the perovskite manganites is determined by spin-spin (exchange) interactions between the Mn^{3+} and Mn^{4+} ions and so is unrelated to any spin-lattice processes. In all cases studied, the linewidth ΔH away from magnetic and structural transitions can be fitted to a simple expression [30-32]

$$\Delta H = [C/T\chi_{dc}(T)]\Delta H(\infty), \quad (5)$$

where $\Delta H(\infty)$ is system dependent constant, and may be identified with the high-temperature limit of the linewidth. Using the relation $I \propto \chi_{esr} \sim \chi_{dc}$, one can easily deduce that the production of $\Delta H \times I$ is in proportion to the inverse temperature. Figure 6 shows the plots of $\Delta H \times I$ vs $1000/T$. Departing from the critical regime, a linear behavior is clearly observed. The result is in good agreement with spin-only relaxation mechanism.

In summary, we demonstrate that the mapping of EPR parameters offers a powerful tool to investigate high-temperature spin dynamics in the phase diagram of CMR manganites. An electron-hole asymmetry of g factor is linked to the different ground states in LCMO phase diagram. The narrowing behavior of linewidth ΔH and peaking behavior of activation energy ΔE as a function of x reveal the strong FM coupling at $x = 3/8$. The analysis of linewidth ΔH and intensity I supports that the EPR signal originates from the magnetic clusters, dominated by spin-spin exchange interaction.

This work was supported by the National Nature Science Foundation of China and the National Basic Research Program of China.

References

1. E. Dagotto, *Science* **309**, 257 (2005).
2. A. J. Millis, *Nature* **392**, 147 (1998).
3. Y. Tokura and N. Nagaosa, *Science* **288**, 462 (2000).
4. P. Schiffer, A. P. Ramirez, W. Bao, and S-W. Cheong, *Phys. Rev. Lett.* **75**, 3336 (1995); S-W. Cheong and H. Y. Hwang, in *Colossal Magnetoresistive Oxides*, edited by Y. Tokura (Gordon and Breach Science Publishers, New York, 2000); see also K. H. Kim, M. Uehara, V. Kiryukhin, and S-W. Cheong, in *Colossal Magnetoresistive Manganites*, edited by T. Chatterji (Kluwer Academic Publishers, Dordrecht, 2004).
5. C. Zener, *Phys. Rev.* **82**, 403 (1951).
6. A. J. Millis, P. B. Littlewood, and B. I. Shraiman, *Phys. Rev. Lett.* **74**, 5144 (1995); A. J. Millis, B. I. Shraiman, and R. Mueller, *Phys. Rev. Lett.* **77**, 175 (1996).
7. Z. Popović and S. Satpathy, *Phys. Rev. Lett.* **88**, 197201 (2002).
8. M. B. Salamon and M. Jaime, *Rev. Mod. Phys.* **73**, 583 (2001).
9. J. M. De Teresa, M. R. Ibarra, P. A. Algarabel, C. Ritter, C. Marquina, J. Blasco, J. García, A. del Moral, and Z. Arnold, *Nature* **386**, 256 (1997).
10. L. Vasiliu-Doloc, S. Rosenkranz, R. Osborn, S. K. Sinha, J. W. Lynn, J. Mesot, O. H. Seeck, G. Preosti, A. J. Fedro, and J. F. Mitchell, *Phys. Rev. Lett.* **83**, 4393 (1999).
11. C. P. Adams, J. W. Lynn, Y. M. Mukovskii, A. A. Arsenov, and D. A. Shulyatev, *Phys. Rev. Lett.* **85**, 3954 (2000).
12. K. H. Kim, M. Uehara, and S-W. Cheong, *Phys. Rev. B* **62**, R11945 (2000).
13. Hongsuk Yi, N. H. Hur, and Jaejun Yu, *Phys. Rev. B* **61**, 9501 (2000).
14. S. B. Oseroff, M. Torikachvili, J. Singley, S. Ali, S. -W. Cheong, and S. Schultz, *Phys. Rev. B* **53**, 6521 (1996).
15. V. A. Ivanshin, J. Deisenhofer, H.-A. Krug von Nidda, A. Loidl, A. A. Mukhin, A. M.

Balbashov, and M. V. Eremin, Phys. Rev. B **61**, 6213 (2000).

16. Janhavi P. Joshi, K. Vijaya Sarathy, A. K. Sood, S. V. Bhat, and C. N. R. Rao, J. Phys.: Condens. Matter **16**, 2869 (2004).

17. A. Abragam and B. Bleaney, *Electron Paramagnetic Resonance of Transition Ions* (Clarendon Press, Oxford, 1970).

18. M. Quijada, J. Černe, J. R. Simpson, H. D. Drew, K. H. Ahn, A. J. Millis, R. Shreekala, R. Ramesh, M. Rajeswari, and T. Venkatesan, Phys. Rev. B **58**, 16093 (1998).

19. K. H. Kim, J. H. Jung, and T. W. Noh, Phys. Rev. Lett. **81**, 1517 (1998).

20. K. H. Kim, S. Lee, T. W. Noh, and S.-W. Cheong, Phys. Rev. Lett. **88**, 167204 (2002).

21. F. Rivadulla, M. A. López-Quintela, L. E. Hueso, J. Rivas, M. T. Causa, C. Ramos, R. D. Sánchez, and M. Tovar, Phys. Rev. B **60**, 11922 (1999).

22. C. Kittel, *Introduction to solid state physics* (7th edition, John Wiley & Sons, inc., New York, 1995).

23. S. E. Lofland, P. Kim, P. Dahiroc, S. M. Bhagat, S. D. Tyagi, S. G. Karabashev, D. A. Shulyatev, A. A. Arsenov, and Y. Mukovskii, Phys. Lett. A **233**, 476 (1997).

24. C. Rettori, D. Rao, J. Singley, D. Kidwell, S. B. Oseroff, M. T. Causa, J. J. Neumeier, K. J. McClellan, S.-W. Cheong, and S. Schultz, Phys. Rev. B **55**, 3083 (1997).

25. A. Shengelaya, G.-M. Zhao, H. Keller, and K. A. Müller, Phys. Rev. Lett. **77**, 5296 (1996).

26. A. Shengelaya, G.-M. Zhao, H. Keller, K. A. Müller, and B. I. Kochelaev, Phys. Rev. B **61**, 5888 (2000).

27. A. I. Shames, E. Rozenberg, G. Gorodetsky, and Ya. M. Mukovskii, Phys. Rev. B **68**, 174402 (2003).

28. D. C. Worledge, L. Miéville, and T. H. Geballe, Phys. Rev. B **57**, 15267 (1998).

29. V. A. Atsarkin, V. V. Demidov, G. A. Vasneva, and K. Conder, Phys. Rev. B **63**, 092405 (2001).

30. M. T. Causa, M. Tovar, A. Caneiro, F. Prado, G. Ibañez, C. A. Ramos, A. Butera, B. Alascio, X. Obradors, S. Piñol, F. Rivadulla, C. Vázquez-Vázquez, M. A. López-Quintela, J. Rivas, Y. Tokura, and S. B. Oseroff, Phys. Rev. B **58**, 3233 (1998).

31. D. L. Huber, G. Alejandro, A. Caneiro, M. T. Causa, F. Prado, M. Tovar, and S. B. Oseroff, Phys. Rev. B **60**, 12155 (1999).

32. M. Tovar, G. Alejandro, A. Butera, A. Caneiro, M. T. Causa, F. Prado, and R. D. Sánchez, Phys. Rev. B **60**, 10199 (1999)

Figure captions

Fig. 1 The Ca doping dependence of XRD patterns for polycrystalline samples of $\text{La}_{1-x}\text{Ca}_x\text{MnO}_3$ ($x = \text{N}/8$, $\text{N} = 1, 2, 3, 4, 5, 6$, and 7) at room temperature.

Fig. 2 EPR spectra of powder samples of $\text{La}_{1-x}\text{Ca}_x\text{MnO}_3$ ($x = \text{N}/8$, $\text{N} = 1, 2, 3, 4, 5, 6$, and 7) at 300 K. The solid lines show the fits of the experimental data to Eq. (1).

Fig. 3 (a) Temperature dependence of the resonance field (H_r) of EPR signals presenting by g factor for $\text{La}_{1-x}\text{Ca}_x\text{MnO}_3$ samples ($x = \text{N}/8$, $\text{N} = 1, 2, 3, 4, 5, 6$, and 7). (b) A false color mapping of g factor in the T vs x plane for $\text{La}_{1-x}\text{Ca}_x\text{MnO}_3$. The solid magenta circles show T_{\min} 's for the measured compositions, and red line is guide to the eye. Dashed line indicates the boundary of two different g -value regimes at $x = 4/8$.

Fig. 4 (a) Temperature dependence of the linewidth ΔH for $\text{La}_{1-x}\text{Ca}_x\text{MnO}_3$ samples ($x = \text{N}/8$, $\text{N} = 1, 2, 3, 4, 5, 6$, and 7). The solid lines correspond to the best fits of Eq. (3). (b) A false color mapping of linewidth ΔH in the T vs x plane for $\text{La}_{1-x}\text{Ca}_x\text{MnO}_3$. The solid magenta circles show T_{\min} 's for the measured compositions, and red line is guide to the eye.

Fig. 5 (a) Doping behavior of the activation energy E_a extracted from temperature dependent EPR linewidth and resistivity for $\text{La}_{1-x}\text{Ca}_x\text{MnO}_3$ system using the adiabatic small polaron model [Eq. (3)]. Solid circle corresponds to the data at $x = 0.2$ obtained by Shengelaya *et al.* [26]. Solid triangles correspond to the data at $x = 0.18, 0.2$, and 0.22 reproduced from Ref. 27. The data obtained by electronic measurements are adapted from Ref. 28. (b) Activation energy ΔE obtained by the fits of double integrated intensity of EPR signals with the Arrhenius law [Eq. (4)].

Fig. 6 The plots of $\Delta H \times I$ vs $1000/T$ showing a linear behavior in the whole doping range.

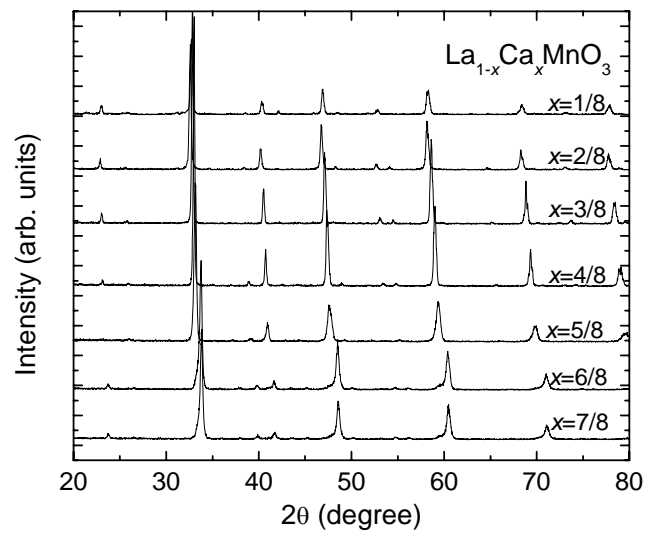


Fig. 1 by Y. Liu *et al.*

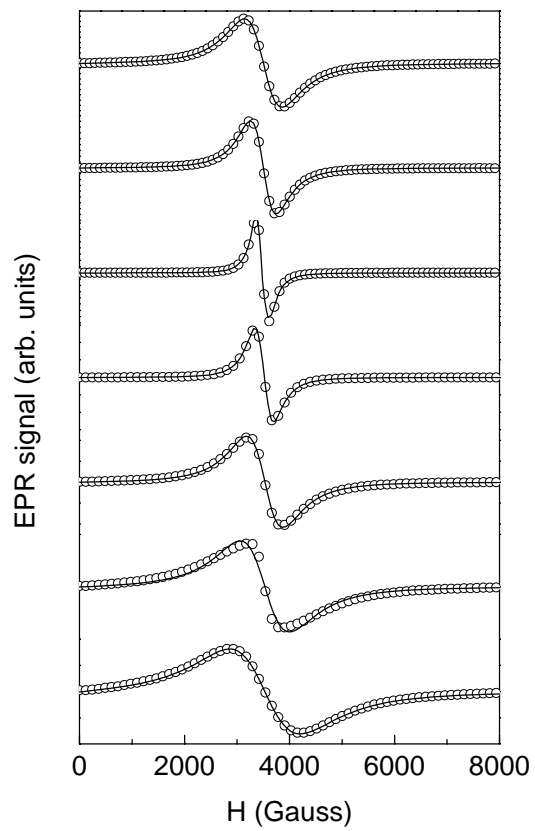


Fig. 2 by Y. Liu *et al.*

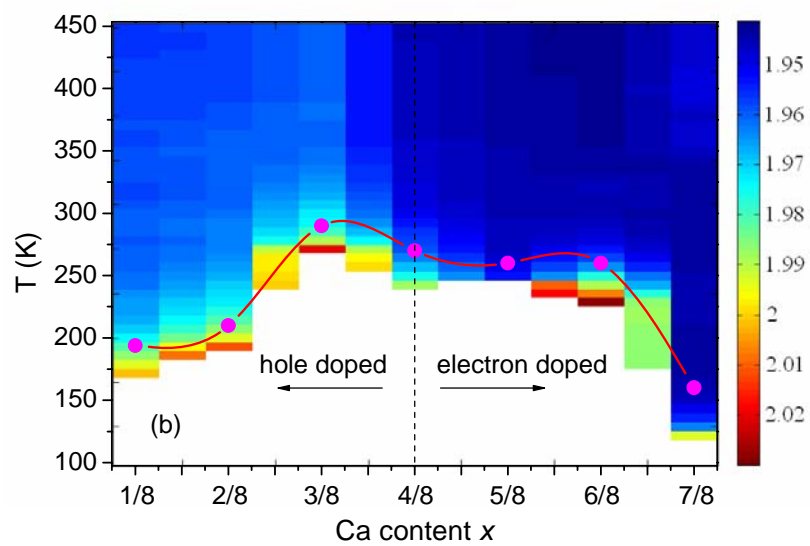
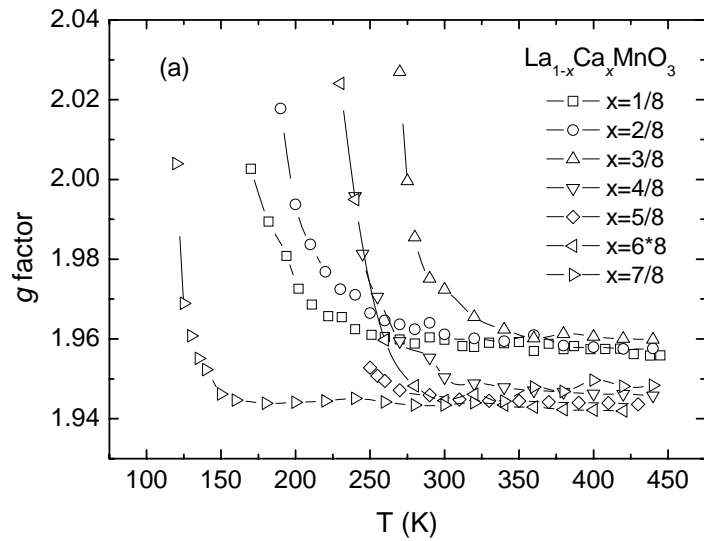


Fig. 3 by Y. Liu *et al.*

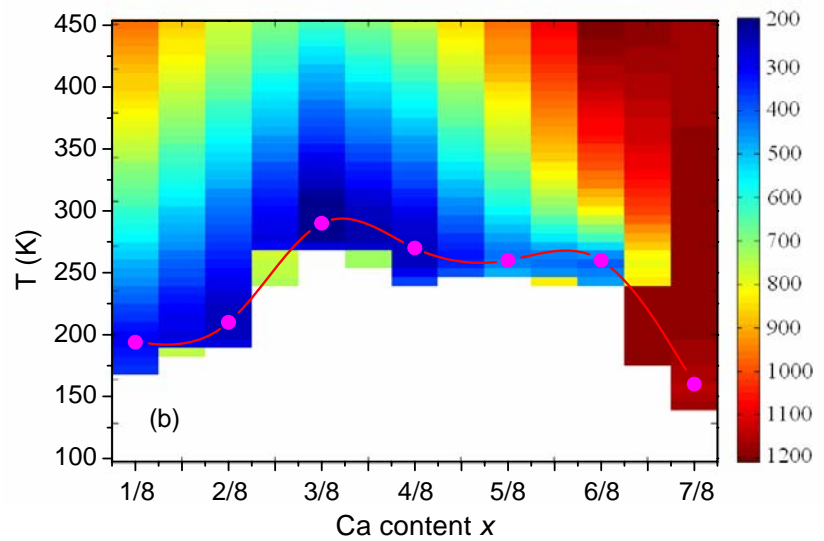
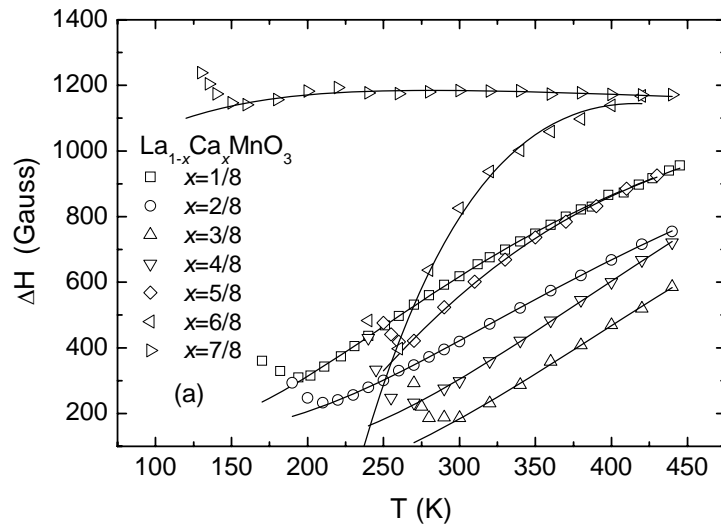


Fig. 4 by Y. Liu *et al.*

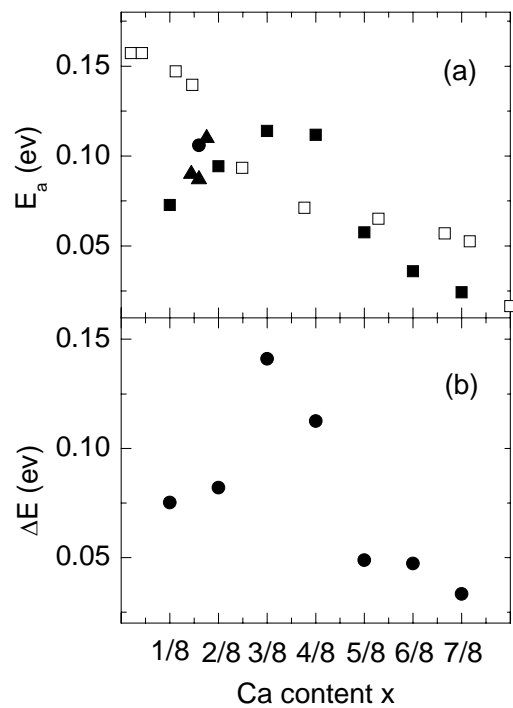


Fig. 5 by Y. Liu *et al.*

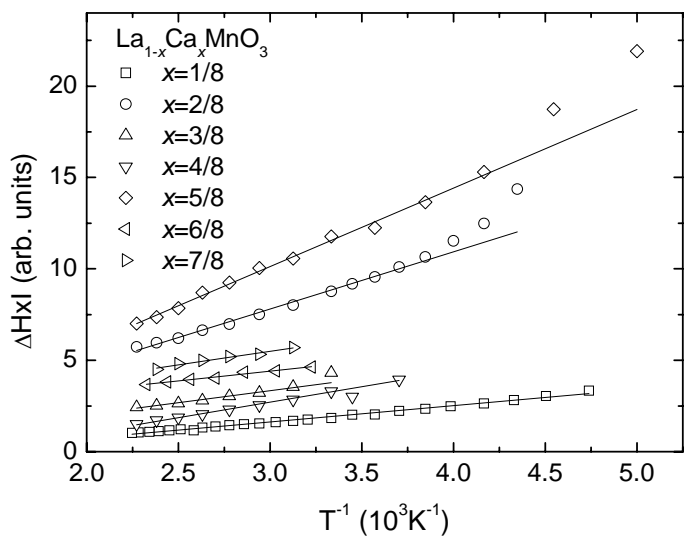


Fig. 6 by Y. Liu *et al.*